

## Chapter 2

# Spring Constant Characterization of a Thermally Tunable MEMS Regressive Spring

Kyle K. Ziegler, Robert A. Lake, and Ronald A. Coutu Jr.

**Abstract** Springs are a widely utilized component in the Microelectromechanical systems (MEMS) industry, especially in inertial devices. Many of these devices rely on the restoring forces of springs to return the device to equilibrium, such as in an accelerometer. By adding external springs with negative spring constant behavior, the total spring constant can be modified. Previous work at AFIT investigated the spring characteristics of a buckled MEMS Si/SiO<sub>2</sub> membrane. This research followed on previous work and attempted to modify the spring behavior. A Ti/Au meander resistor was deposited atop the membrane in an effort to actuate the membrane and change the spring constant. Membrane buckling was investigated through analytical equations and Finite Element analysis (FEA) to predict device behavior. Membrane deflections and thermal effects were measured using an interferometric microscope (IFM) and showed a deflection change of 13.3–22.2  $\mu\text{m}$  in the square style of resistor and 15.1–23.5  $\mu\text{m}$  in the spiral type of resistor. The results concluded that by introducing a thermal stress, the membrane could be actuated with a subsequent change in spring constant. From the initial position to the fully thermally actuated position, we expect the spring to undergo a threefold increase in spring stiffness in the linear region.

**Keywords** MEMS • Buckling • Springs • Thermal actuation

### 2.1 Introduction

Buckling is commonly identified as a type of failure method in a structural member, and it has been studied as far back as the eighteenth century when Euler studied and developed equations describing beam buckling [1]. Buckling occurs within a long but thin structure loaded in compression, which, instead of fracturing, the member drastically bows in one direction. Buckling in macro-scale structures is typically avoided, while buckling in MEMS devices has been utilized in numerous applications. It can be used in devices to maintain a specific position without input power, such as in memory [2]. It has been used in the domain of microfluidics for valve mechanisms [3, 4], and it can be used for actuators [5].

Recently, buckling in MEMS has been used for its ability to display linear regressive spring constant behavior [6], which can be explained by the following. Suppose that a buckled membrane is loaded normal to the planar surface. The membrane deflects in the direction opposite of the buckling. This deflection causes the spring constant of the structure to change. Initially, the membrane resists deflection, similar to a normal compressive spring with linear behavior [7]. Upon reaching a certain deflected distance, the membrane will begin to require a linearly decreasing load i.e. less force required for further deflection. The goal of this research is to demonstrate that by thermally increasing the post-buckled deflection, the spring constant of the structure will increase.

---

**Disclaimer:** The views expressed in this article are those of the authors and do not reflect the official policy or position of the United States Air Force, Department of Defense, or the U.S. Government.

K.K. Ziegler • R.A. Lake • R.A. Coutu Jr. (✉)  
Air Force Institute of Technology, 2950 Hobson Way, Bldg 641, Wright-Patterson AFB, OH 45433, USA  
e-mail: [Ronald.Coutu@afit.edu](mailto:Ronald.Coutu@afit.edu)

## 2.2 Design

At the root of the design is the buckled membrane, for which Silicon on Insulator (SOI) is used. The joint silicon (Si) and silicon dioxide ( $\text{SiO}_2$ ) buckles when the supporting handle wafer is etched away. The compressive stresses required for buckling are characteristic to SOI and formed during fabrication. In this process, the device layer is bonded at high temperatures, and once cooled; the difference in coefficients of thermal expansion generates large internal planar stresses [8]. As a result,  $\text{SiO}_2$  contains high compressive stress ( $>200$  MPa), but the surrounding silicon is lightly stressed due in part to the high modulus of elasticity and low coefficient of thermal expansion.

When transversely displaced, the buckled membrane displays linear regressive spring constant behavior. Shown in Fig. 2.1a, b, the buckled membrane's spring characteristics are shown with the corresponding location during actuation. By thermally stressing, and subsequently, straining the membrane, this research seeks to increase the displacement of the membrane from the initial buckled position. With the increased deflection, the membrane will display modified spring characteristics, shown in Fig. 2.1c.

In order to introduce thermal stress to the membrane, current was passed through a deposited resistor which transfers heat energy to the membrane in the form of joule heating. Two styles of resistor were used in this research. The first resistor design (Fig. 2.2a) consisted of straight edges and sharp corners. The purpose of this resistor was to quickly fabricate and test a design, to provide a high heater surface area, and to reach a maximum temperature with under 25 V applied. Additionally, the total resistance from pad to pad is calculated to be  $1.07 \times 10^{-5} \Omega$ . Also shown in Fig. 2.2a are a series of four bars that surround the filament area, these did not affect the resistor performance, and they were used only to align the resistor mask when designing.

The second resistor style (Fig. 2.2b) was designed in a spiral shape to reduce current concentration around corners, a concern with the first style of resistor [9]. The design included a thinner filament with increased filament spacing and a total resistance of  $1.05 \times 10^{-4} \Omega$ . These two styles enabled us to determine if a difference in filament thickness or spacing could be a factor in heater performance. Additionally, this research focused solely on testing the capabilities of joule heating on a buckled membrane, and minimizing power consumption for packaging and incorporating into MEMS devices will be left to future research.

The resistors were fabricated atop the membrane prior to buckling. In the following section, the fabrication procedures are outlined.

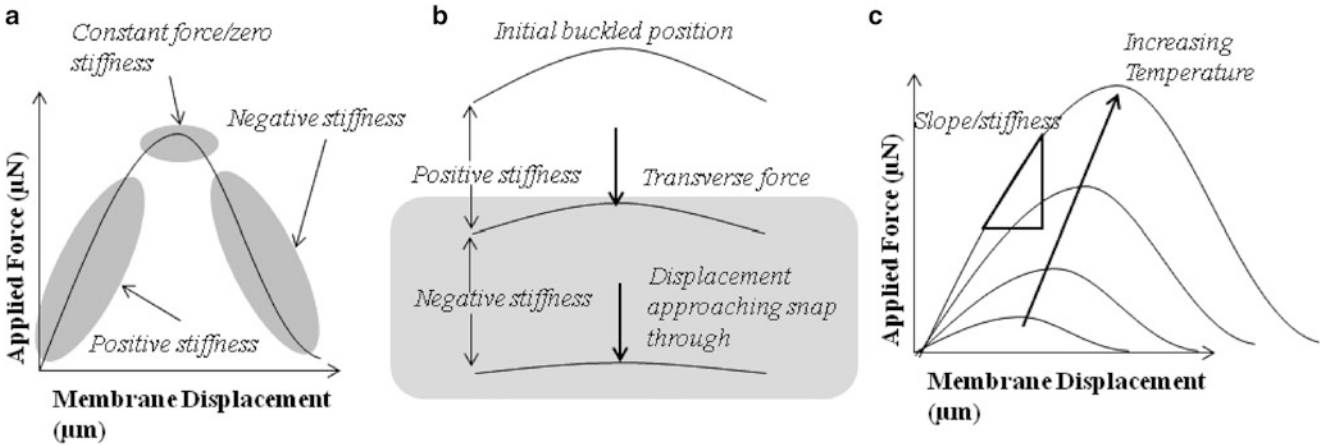


**Fig. 2.1** (a) Schematic of the measured force response from a incrementally displaced membrane. (b) Cross-sectional view of buckled membrane actuation. (c) Predicted effect to force response from thermal actuation

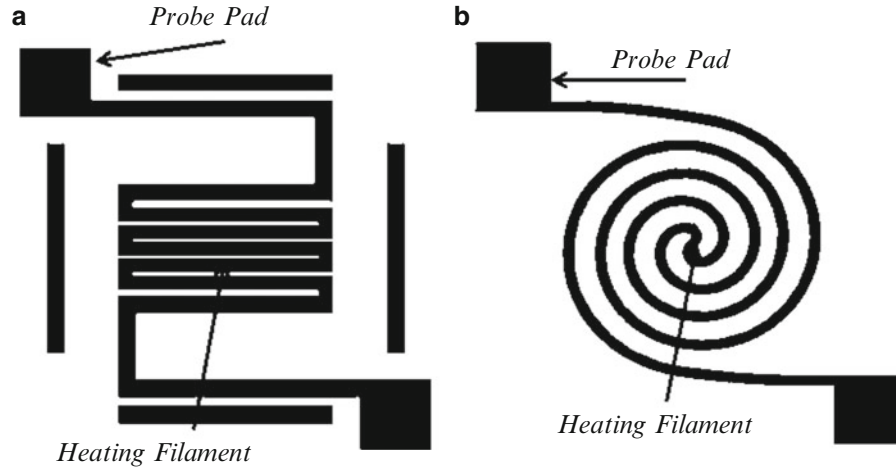


**Fig. 2.2** (a) Square meander resistor design. (b) Spiral resistor design

## 2.3 Fabrication

A two mask process is required for the device fabrication. One mask is required for the topside resistors, and another is needed for backside etch holes. The resistors are deposited atop an SOI wafer with a 5  $\mu\text{m}$  device layer and a 2  $\mu\text{m}$  oxide layer for optimal buckling characteristics, namely the degree of internal residual stress.

### 2.3.1 Resistor Fabrication

The process begins with the application of a single layer of SF11 photoresist followed by a single layer of 1818 photoresist, both of which mask the resistor shape (Fig. 2.3a). 1818 is exposed using an MJB3 mask aligner to define the resistor locations. 1818 is further used to mask the SF11 layer below which is exposed in a deep ultra violet (DUV) flood exposure system. SF11 undercuts the 1818 layer (Fig. 2.3b) preventing connection of the sacrificial gold and resistor gold, and ensuring the success of the lift-off technique for unwanted gold removal.

Once SF11 has been exposed, and following a brief develop procedure, bare silicon is exposed in locations where the resistors will be deposited. To do this, gold is evaporated over the surface of the sample, depicted in Fig. 2.3c. The samples are now ready for the backside etching process.

### 2.3.2 Backside Etch Process

The thick side (handle) portion of the sample is patterned using SU-8 photoresist to protect areas where etching is undesired. This design consists of a series of one millimeter squares and circles patterned using manufacturer specified photoresist deposition, exposure, and develop times and temperatures.

After the photoresist processing step, the bulk silicon is rapidly and anisotropically etched using the deep reactive ion etching (DRIE) method. Etching selectivity permits using the oxide layer as a natural etch stop. The resultant structure contains a thin layer of both Si and  $\text{SiO}_2$  which buckles out of plane upon etch completion. The complete process is shown in Fig. 2.4.

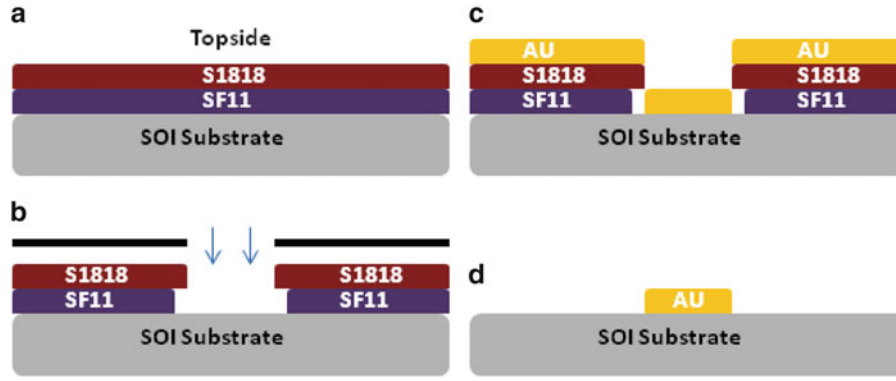


**Fig. 2.3** Resistive heating element deposition process. (a) Initial photoresist spin-on, (b) ultraviolet (UV) light exposure and develop, (c) gold deposition through electron beam evaporation, (d) excess gold and photoresist removal

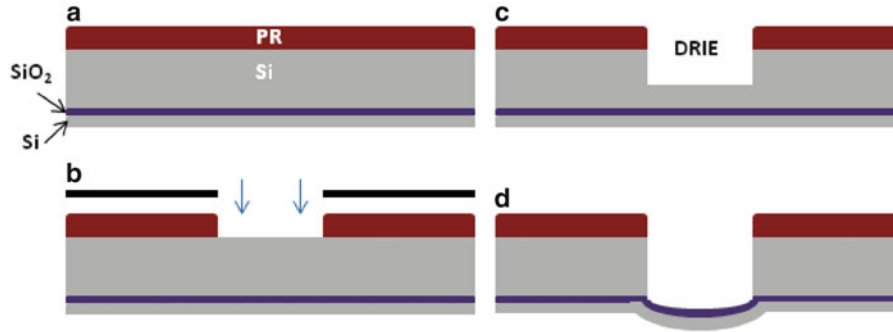


**Fig. 2.4** Backside etch process. (a) Initial sample, (b) SU-8 photoresist deposition and patterning, (c) DRIE process, (d) instantaneous membrane buckling upon etch completion

## 2.4 Modeling and Simulation

Timoshenko and Gere established equations for modeling multiple geometric buckling scenarios [10]. Here the strain energy method is utilized for estimating buckling. Through this method, the outward deflection of the membrane is found by minimizing the strain energy of the system. These equations consider the energy generated by both the strain energy of bending and the work done by the compressive forces during buckling.

Popescu et al. simplified the mathematical expressions provided by Timoshenko and Gere and formed equations used to estimate the deflection in a buckled structure [11]. Adding the two energy equations, solving the integrals, and simplifying these equations results in the total strain energy of the membrane which is represented by Eq. 2.1.

*Equation 2.1 Total Strain Energy*

$$U = 33 \frac{Dh^2}{a^2} \left( \frac{W_o}{h} \right)^4 + 100 \frac{Dh^2}{a^2} \left( \frac{W_o}{h} \right)^2 \left( 1 - \frac{\sigma}{\sigma_{cr}} \right) \quad (2.1)$$

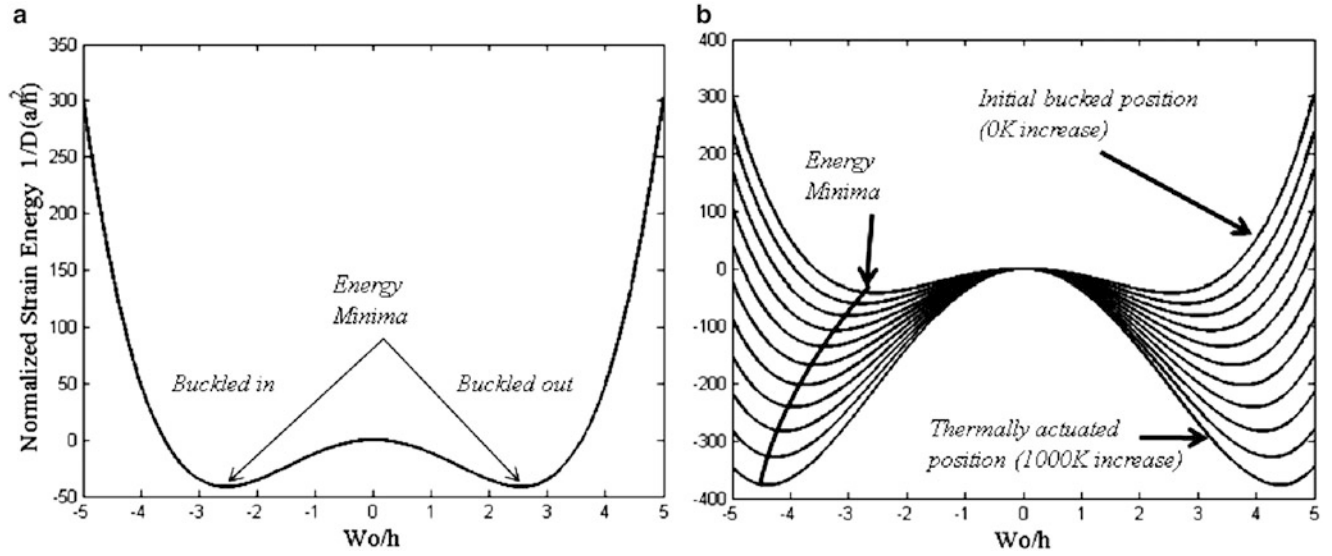


**Fig. 2.5** (a) Initial energy curve for the buckled Si/SiO<sub>2</sub> membrane. The local minima indicate locations of buckled equilibrium. (b) Successive energy curves corresponding to increased temperature in the membrane

Where  $W_o$  is the center deflection,  $h$  is the thickness,  $a$  and  $b$  are the length and width,  $\sigma_x$  and  $\sigma_y$  are the compressive stresses, and  $D$  is the flexural rigidity represented by Eq. 2.2

Equation 2.2 Flexural rigidity

$$D = \frac{Eh^3}{12(1 - \nu^2)} \quad (2.2)$$

This equation can be plotted to visually show the expected amount of deflection in the membrane. Figure 2.5a graphically illustrates Eq. 2.1 with the appropriate material properties used in the equation.

Thermal behavior is studied in this thesis, and Eq. 2.1 can be modified to include thermal stresses. By adding thermal stress (Eq. 2.3) to the total stress ( $\sigma$ ), Eq. 2.1 accommodates for the addition of heat to the buckled membrane.

Equation 2.3 Thermal stress

$$\sigma_{therm} = -E_{eff}\alpha_{eff}(T - T_{\infty}) \quad (2.3)$$

This effect is shown in Fig. 2.5b, with each energy curve representing a 100 K increase in temperature.

Using Fig. 2.5a we predict the membrane will initially buckle with 18  $\mu\text{m}$  of deflection, and with Fig. 2.5b we can predict the membrane will actuate upward with a decreasing change in deflection to 30  $\mu\text{m}$  predicted at the maximum temperature reached by resistive heating.

While analytical equations can determine the profile and the degree of deflection in the membrane, advanced modeling is necessary to understand transverse loading, heat transfer, and the electro-thermal behavior. Through finite element analysis (FEA) techniques, stress, strain, temperature, fluid flow, deflection, electrical characteristics, and other analyses can be performed for unusually shaped or loaded objects.

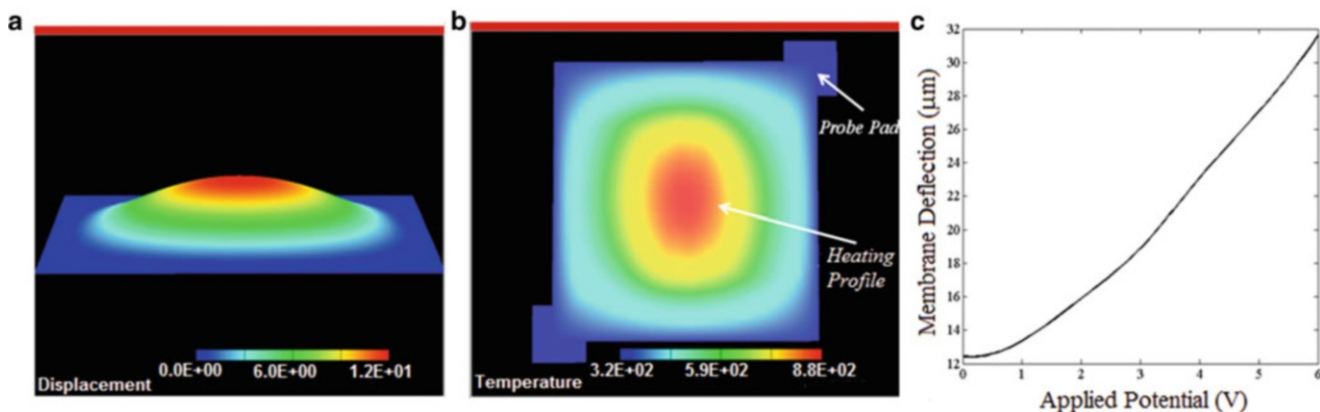


**Fig. 2.6** (a) Initial buckling shape and deflected distance. (b) Heating profile with an applied voltage across the resistor. (c) Membrane buckling deflection distance with thermal influence

### 2.4.1 Finite Element Analysis (FEA)

CoventorWare<sup>®</sup> is a finite element analysis (FEA) software tool which assists MEMS researchers by using familiar processes to create models for FE analysis. Users specify material properties, create a design layout, and develop a process as if the device were to be fabricated. The system compiles this information and provides the user with a three-dimensional rendition (solid model) of the device. It is at this step where the user decides the type and style of the finite elements (mesh). After generating a mesh, the user can select from a comprehensive suite of solvers, each focused on a specific area of MEMS. Within these, boundary and loading conditions are specified to closely approximate device behavior.

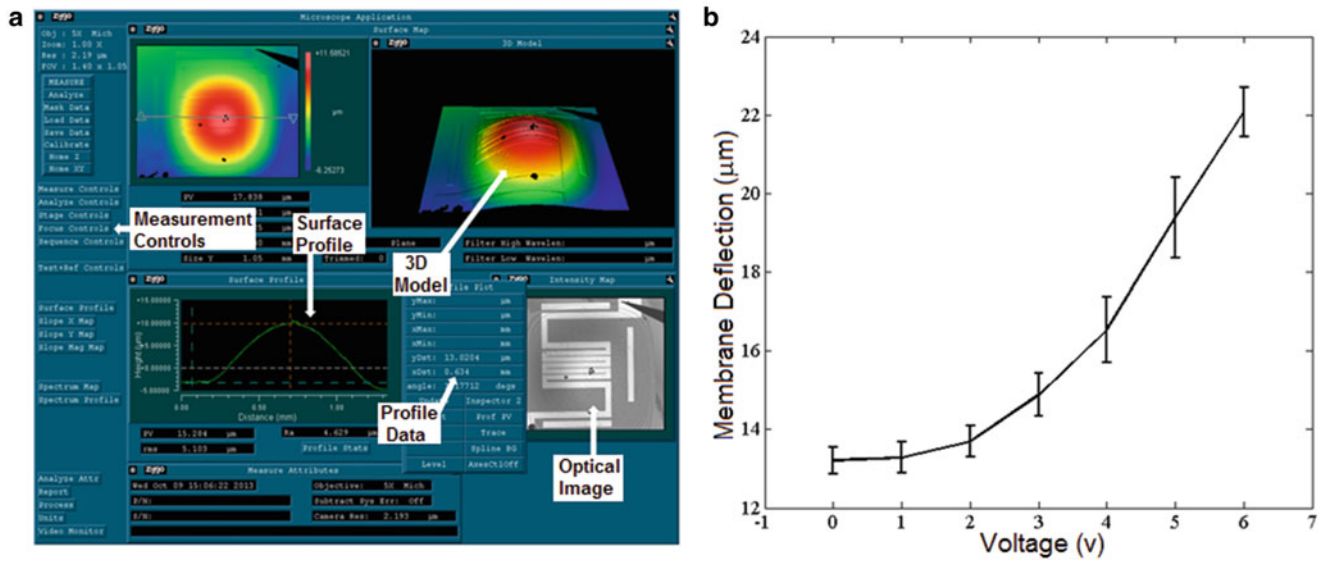
For this research, a flat plate with rigid edges is used to model the membrane. Initial membrane buckling was modeled first with thermal effects added in later simulations. Next, resistor heating with applied voltage values was used in conjunction with the temperature model to determine the thermal effects. Visual depictions of the initial buckling, thermal profile, and the expected membrane actuation with applied voltages are shown in Fig. 2.6.

Figure 2.6a shows the result of the compressive stress in the membrane at room temperature. Figure 2.6b shows the membrane with only an applied voltage to the probe pads. This illustrates the maximum temperature expected in the membrane at 6 V (1,200 K) and the temperature gradient from the center to the edges. Figure 2.6 is not color coded to show different materials, but the gold resistor is included and can be seen overhanging the membrane corner. Finally, in Fig 2.6c the temperature is applied to the original membrane model to simulate the effects of thermal stress. FEA predicts the deflection of the membrane to range from 12.4  $\mu\text{m}$  of initial deflection to 31.6  $\mu\text{m}$  with 6 V of applied voltage.

## 2.5 Experimental Results and Testing

In order to determine the vertical displacement from the thermal effects, the devices were measured under a white light interferometric microscope (IFM). The Zygo<sup>®</sup> IFM is equipped with movable probes which can be connected to a power supply in order to supply the necessary input voltages and measure micro scale devices. The IFM user interface screen (shown in Fig. 2.7a) provides the user with an optical image to aid with microscope focusing, a top view contour image showing the vertical displacements, a three-dimensional model generated from the microscope image, and a cross-sectional image showing the surface profile. In this research, the probes were connected to a 25 V power supply, in which 0–6 V were used, and carefully lowered to the contact pads, after which power was applied to the probes. Prior to making contact with the probe tips, the Zygo<sup>®</sup> table was first positioned for optimal focus. Measurements were then taken by manually adjusting the applied voltage and measuring the deflection in the membrane. The deflections were recorded for 0–6 V across twenty samples.





**Fig. 2.7** (a) Zygo® user interface screen. (b) Average measured deflection data for the square resistor mounted on the membrane at 0–6 V applied

Once tested, the displacements at each voltage were plotted, and the average of 20 separate devices was recorded. The square meander resistor increased from an initial deflection of 13.3–22.2  $\mu\text{m}$  (Fig. 2.7b), and the spiral resistor deflected from an initial displacement of 15.1–23.5  $\mu\text{m}$ . Each resistor maintained a different respective voltage limit before resistor failure as well as a different deflected distance. The average square meander resistor failed at 6 V and the spiral resistor failed at 8 V. The resistor failure was caused by the gold melting and failing to provide an electrical connection, and the voltage at which it failed was defined by the individual resistance of the resistor. Furthermore, the major focus of this research was to have the resistor heat the membrane and cause further deflection, and the resistor was only driven to failure to observe the maximum heating potential.

Referring back to the models, analytical modeling consistently overestimated membrane deflection by 30 % and FEA underestimated initial buckling by 6 % and overestimated maximum actuation by 35 %. The cause of the discrepancy stems from the assumptions made in the models. Analytical models do not take into consideration the bending effect of the gold film, which reduce the overall buckling distance. Furthermore, FEA assumes a perfectly fixed edge, and idealizes the probe-probe pad contact.

Using this information in conjunction with the derivative of Eq. 2.3, the force/deflection characteristics of the membrane were estimated. The stress value in the equation was modified to reflect the actual membrane deflection at each voltage. The result, illustrated in Fig. 2.8, shows the characteristics of the force/deflection curve, and in particular, the change in stiffness of the different membranes.

The membrane initial equilibrium position is indicated by the “membrane displacement” label on the figure, and through transverse actuation, the membrane will follow the curve traveling from right to left. Each curve corresponds to a different voltage applied to the resistor, and within each curve, the returning force from the membrane at each deflected position is indicated by the vertical axis. Because of this, the slope of this line is indicative of the stiffness of the membrane. In this plot, the equation predicts a threefold increase of membrane stiffness. This change in membrane stiffness could be useful in a wide array of MEMS devices, in particular for tuning the characteristics of inertial devices. Additionally, the linear regressive characteristics, in particular the negative stiffness region could be used as stiffness offset. Further research should investigate scaling this device to useful sizes, and implementing this structure in a current MEMS device.

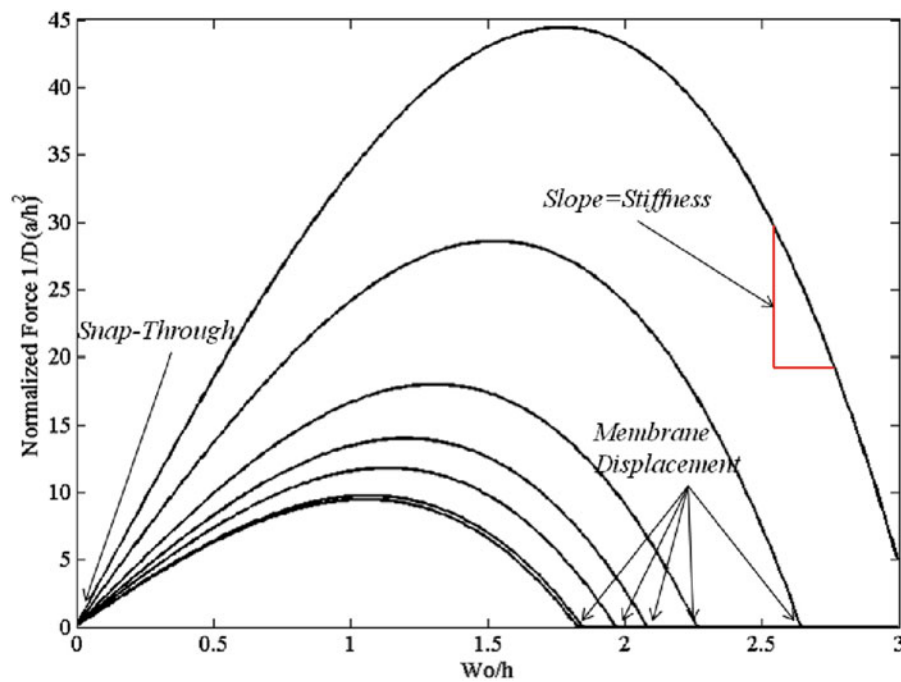


**Fig. 2.8** Analytically determined force/deflection behavior. The original membrane displacement is indicated on the x-axis, and the slope of the curves is directly correlated to the stiffness of the membrane

## 2.6 Conclusion

A buckled membrane formed from Si and SiO<sub>2</sub> was thermally actuated in order to test its capabilities as a tunable spring. Two types of deposited resistors were used to provide the thermal energy to the membrane, a square meander and a spiral resistor. Both analytical and finite element methods were used to model the behavior of the membrane under applied thermal effects. The membrane was fabricated using conventional cleanroom processes, and tested under an IFM to measure the degree of deflection. Experimental deflection values were determined to be different from the model's prediction because of the assumptions made in the modeling process. Finally, the measured deflection values were used with the analytical model to estimate the change in spring constant with thermal effects.

**Acknowledgments** The authors would like to thank the Air Force Research Laboratory (AFRL) Sensors and Propulsion Directorates for their assistance, use of their resources, and facilities. The authors also thank the technical support and dedicated work of AFIT's own cleanroom staff, Rich Johnston and Thomas Stephenson.

## References

1. Brush DO, Almroth BO (1975) Buckling of bars, plates, and shells. McGraw-Hill, New York
2. Hälgl B (1990) On a micro-electro-mechanical nonvolatile memory cell. IEEE Trans Electron Devices 37(10):2230–2236
3. Wagner B, Quenzer HJ, Hoerschelmann T, Lisec T, Juerss M (1996) Bistable microvalve with pneumatically coupled membranes. In: Micro electro mechanical systems, San Diego
4. Jerman H (1994) Electrically-activated, normally-closed diaphragm valves. J Micromech Miroeng 4:210–216
5. Lin L, Lin S-H (1998) Vertically driven microactuators by electrothermal buckling effects. Sens Actuators A 71:35–39
6. Starman LA, Coutu RA (2012) Using micro-Raman spectroscopy to assess MEMS Si/SiO<sub>2</sub> membranes exhibiting negative spring constant behavior. J Exp Mech 53:593–604
7. Almen JO, Laszlo A (1936) The uniform-section disk spring. Am Soc Mech Eng 58:305–314



8. Kaltsas G, Nassiopoulou A, Siakavellas M, Anastassakis E (1998) Stress effect on suspended polycrystalline silicon membranes fabricated by micromachining of porous silicon. *Sens Actuators* 68(1–3):429–434
9. Coutu RA, Ostrow SA (2013) Microelectromechanical systems resistive heaters as circuit protection devices. *IEEE Trans Compon Packaging Manuf Technol* 3(12):2174–2179
10. Timoshenko SP, Gere JM (1961) *Theory of elastic stability*. McGraw-Hill, New York
11. Popescu DS, Lammerink SJ, Elwenspoek M (1994) Buckled membranes for microstructures. In: *IEEE workshop on micro electro mechanical systems*, Oiso

MEMS and Nanotechnology, Volume 8  
Proceedings of the 2014 Annual Conference on  
Experimental and Applied Mechanics  
Prorok, B.C.; Starman, L.; Hay, J.; Shaw III, G. (Eds.)  
2015, VII, 83 p. 67 illus., Hardcover  
ISBN: 978-3-319-07003-2